

POLARIZED PARTON DISTRIBUTIONS IN LIGHT-FRONT DYNAMICS

P. Faccioli

ECT, Villa Tambosi, 38050 Villazzano,
(Trento), Italy
E-mail: faccioli@ect.it*

F. Cano

*Dipartimento di Fisica, Università degli Studi di Trento,
I-38050 Povo (Trento) Italy
E-mail: cano@science.unitn.it*

M. Traini

*Dipartimento di Fisica, Università degli Studi di Trento,
and Istituto Nazionale di Fisica Nucleare, G.C. Trento
I-38050 Povo (Trento) Italy
E-mail: traini@science.unitn.it*

V. Vento

*Departament de Física Teòrica, Universitat de València
and Institut de Física Corpuscular, Centre Mixt Universitat de València,
Consejo Superior de Investigaciones Científicas,
E-46100 Burjassot (València) Spain
E-mail: vicente.vento@uv.es*

We present a consistent calculation of the structure functions within a light-front constituent quark model of the nucleon. Relativistic effects and the relevance of the covariance constraints are analyzed for polarized parton distributions. Various models, which differ in their gluonic structure at the hadronic scale, are investigated. The results of the full covariant calculation are compared with those of a non-relativistic approximation to show the structure and magnitude of the differences. It is also shown how measurements of transversity in doubly polarized Drell-Yan lepton pair production are a clearcut sign of covariance requirements for the spin.

1 Introduction

We report here on calculations of the polarized structure functions within a covariant quark model of the nucleon. The framework used is based on a quark-parton picture we have developed to describe the structure on the nucleons in the deep inelastic regime¹. The central assumption in this procedure² is the existence of a scale, μ_0^2 , where the short range (perturbative) part of the interaction is negligible, therefore the glue and sea are suppressed, and the

long range (confining) part of the interaction produces a proton composed of three (valence) quarks only. Jaffe and Ross³ proposed thereafter, to ascribe the quark model calculations of matrix elements to that hadronic scale μ_0^2 . For larger Q^2 their Wilson coefficients will give the evolution as dictated by perturbative QCD. In this way quark models, summarizing a great deal of hadronic properties, may substitute *ad hoc* low-energy parameterizations.

However, it has been quite evident, since the original formulation of many of these models, that relativistic effects to the nucleon wave function, as well as covariance requirements, are needed even for a phenomenological description of the structure of hadrons. To accomplish with this aim we develop a constituent quark model in the light-front realization of the Hamiltonian dynamics where covariance can be incorporated in a rather transparent and elegant manner⁴.

We apply this formalism to the calculation of polarized parton distribution. The role of initial soft gluons in the description of the parton distribution (and especially gluon polarization) is analyzed. Finally we show how differences between transverse and longitudinal polarization are a direct consequence of a light-front treatment of the spin and they may be detected experimentally in a rather model independent way.

2 Polarized parton distributions at the hadronic scale

The parton distributions at the hadronic scale μ_0^2 are assumed to be valence quarks and gluons. We will introduce the gluons later on in a phenomenological way, let us therefore now restrict our discussion to the quarks. The quark distribution is determined by the quark momentum density¹,

$$q_V^{\uparrow(\downarrow)}(x, \mu_0^2) = \frac{1}{(1-x)^2} \int d^3k n_q^{\uparrow(\downarrow)}(\mathbf{k}^2) \delta\left(\frac{x}{1-x} - \frac{k^+}{M_N}\right), \quad (1)$$

where $k^+ = \sqrt{\mathbf{k}^2 + m_q^2} + k_z$ is the light-cone momentum of the struck parton, M_N and m_q are the nucleon and (constituent) quark masses respectively and $n_q^{\uparrow}(\mathbf{k}^2)$, $n_q^{\downarrow}(\mathbf{k}^2)$ represent the density momentum distributions of the valence quark of q -flavor *aligned* (\uparrow) or *anti-aligned* (\downarrow) to the total spin of the parent nucleon.

$$n_{u(d)}^{\uparrow(\downarrow)}(\mathbf{k}^2) = \langle N, J_z = +1/2 | \sum_{i=1}^3 \frac{1 + (-)\tau_i^z}{2} \frac{1 + (-)\sigma_i^z}{2} \delta(\mathbf{k} - \mathbf{k}_i) | N, J_z = +1/2 \rangle. \quad (2)$$

The distributions (2) have been evaluated in the past making use of non-relativistic constituent quark models while, in the present investigation, we

want to improve their description by including relativistic effects as dictated by a light-front formulation of a three-body interacting system.

We just outline here the basic features of this formulation (see ⁵ for a review). In light-front dynamics the intrinsic momenta of the constituent quarks (k_i) can be obtained from the corresponding momenta (p_i) in a generic reference frame through a light-front boost ($k_i = \mathcal{L}_f^{-1}(P_{\text{tot}}) p_i$, $P_{\text{tot}} \equiv \sum_{i=1}^3 p_i$) such that the Wigner rotations reduce to identities. The spin and spatial degrees of freedom are described by the wave function:

$$\Psi = \frac{1}{\sqrt{P^+}} \delta(\tilde{P} - \tilde{p}) \chi(\mathbf{k}_1, \mu_1, \dots, \mathbf{k}_3, \mu_3) \quad (3)$$

where μ_i refer to the eigenvalue of the light-front spin, so that the spin part of the wave function is transformed by the tensor product of three independent Melosh rotations: $R_M^\dagger(\mathbf{k}_i, m_i)$ ⁶, namely $\mathcal{R}^\dagger = \prod_{\otimes, i=1}^3 R_M^\dagger(\mathbf{k}_i, m_i)$. Finally, the internal wave function is an eigenstate of the baryon mass operator $M = M_0 + V$, with $M_0 = \sum_{i=1}^3 \omega_i = \sum_{i=1}^3 \sqrt{\mathbf{k}_i^2 + m_i^2}$, where the interaction term V must be independent on the total momentum \tilde{P} and invariant under rotations.

In the present work we will discuss results of a confining mass equation of the following kind

$$(M_0 + V) \psi_{0,0}(\xi) \equiv \left(\sum_{i=1}^3 \sqrt{\mathbf{k}_i^2 + m_i^2} - \frac{\tau}{\xi} + \kappa_l \xi \right) \psi_{0,0}(\xi) = M \psi_{0,0}(\xi) , \quad (4)$$

where $\sum_i \mathbf{k}_i = 0$, $\xi = \sqrt{\vec{\rho}^2 + \vec{\lambda}^2}$ is the radius of the hyper-sphere in six dimension and $\vec{\rho}$ and $\vec{\lambda}$ are the intrinsic Jacobi coordinates $\vec{\rho} = (\mathbf{r}_1 - \mathbf{r}_2)/\sqrt{2}$, $\vec{\lambda} = (\mathbf{r}_1 + \mathbf{r}_2 - 2\mathbf{r}_3)/\sqrt{6}$. The choice of the mass operator (4) has been motivated by the fact that it combines a simple form with a reasonable description of the baryonic spectrum ^{7,8}.

The intrinsic wave function (disregarding the color part) of the nucleon can be written:

$$|N, J, J_n = +1/2\rangle = \psi_{0,0}(\xi) \mathcal{Y}_{[0,0,0]}^{(0,0)}(\Omega) [\chi_{MS} \phi_{MS} + \chi_{MA} \phi_{MA}] / \sqrt{2} \quad (5)$$

where $\psi_{\gamma,\nu}(\xi)$ is the hyper-radial wave function solution of Eq. (4), $\mathcal{Y}_{[\gamma,l_\rho,l_\lambda]}^{(L,M)}(\Omega)$ the hyper-spherical harmonics defined in the hyper-sphere of unitary radius, and ϕ and χ the flavor and spin wave function of mixed $SU(2)$ symmetry. Let us note that, in order to preserve relativistic covariance, the spin wave

functions

$$\chi_{MS} = \frac{1}{\sqrt{6}} [2 \uparrow\uparrow\downarrow - (\uparrow\downarrow + \downarrow\uparrow) \uparrow] ; \quad \chi_{MA} = \frac{1}{\sqrt{2}} (\uparrow\downarrow - \downarrow\uparrow) \uparrow , \quad (6)$$

have to be formulated by means of the appropriate Melosh transformation of the i th quark spin wave function, i.e., each individual spin vector must be Melosh-rotated:

$$\chi_i = D^{1/2}[R_M(\vec{k}_i)]\chi_i^c = \frac{(m_i + \omega_i + k_{iz}) - i\vec{\sigma}^{(i)}(\hat{z} \times \vec{k}_{i\perp})}{((m_i + \omega_i + k_{iz})^2 + \vec{k}_{i\perp}^2)^{1/2}} \chi_i^c \quad (7)$$

where χ_i^c are the usual Pauli spinors for the particle i .

The calculation of the helicity distribution at the hadronic scale μ_0^2 can be written, according to the expression (1), as:

$$g_1^a(x, \mu_0^2) = \frac{\pi}{9} \frac{M_N}{(1-x)^2} \int_0^\infty d\vec{k}_\perp^2 n(\tilde{k}_z^2, \vec{k}_\perp^2) \frac{B_a \left(m + M_N \frac{x}{(1-x)}\right)^2 + C_a \vec{k}_\perp^2}{\left(m + M_N \frac{x}{(1-x)}\right)^2 + \vec{k}_\perp^2} D(\tilde{k}_z, x) \quad (8)$$

where

$$D(\tilde{k}_z, x) = \frac{M_N \frac{x}{(1-x)} - \tilde{k}_z}{\left|M_N \frac{x}{(1-x)} - 2\tilde{k}_z\right|} \quad (9)$$

$$\tilde{k}_z(x, \vec{k}_\perp^2) = \frac{M_N}{2} \left[\frac{(\vec{k}_\perp^2 + m^2)}{M_N^2} \frac{1-x}{x} - \frac{x}{(1-x)} \right] \quad (10)$$

and $n(\tilde{k}_z^2, \mathbf{k}_\perp^2)$ is the total (unpolarized and flavorless) momentum density distribution of the valence quarks in the nucleon calculated making use of the eigenfunction ψ_{00} of Eq. (4) and properly normalized to the number of particles. The coefficients B_a and C_a take the values $B_u = -C_u = 4$ and $B_d = -C_d = -1$.

The mass equation (4) has been solved numerically by fitting the parameters of the potential to reproduce the basic features of the (non strange) baryonic spectrum up to ≈ 1500 MeV, namely the position of the Roper resonance and the average value of the 1^- states. We obtain⁴: $\tau = 3.3$ and

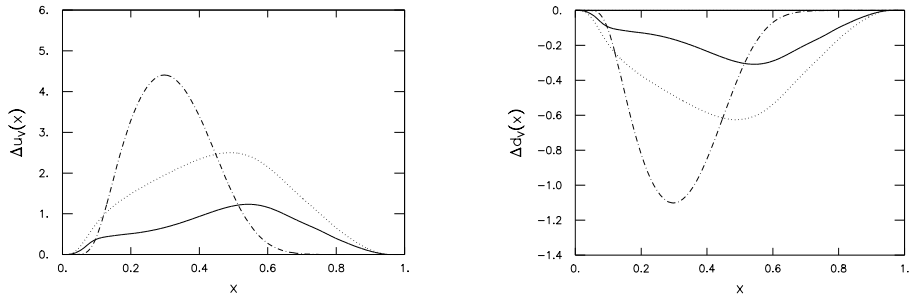


Figure 1: Left panel (Fig. 1a): the polarized distribution $\Delta u_V(x, \mu_0^2)$ as a function of x : the non-relativistic approximation (dot-dashed curve), and the relativized solution of Eq.(4) which neglects Melosh rotations (dotted curve) are compared with the results of a complete light-front calculation (full curve). On the right panel (Fig. 1b) the distribution $\Delta d_V(x, \mu_0^2)$ (same notation).

$\kappa_l = 1.8 \text{ fm}^{-2}$, to be compared with the corresponding non-relativistic ⁷ fit $\tau = 4.59$ and $\kappa_l = 1.61 \text{ fm}^{-2}$. The constituent quark masses have been chosen $m_u = m_d = m_q = M_N/3$.

An important outcome of this relativistic treatment is the large amount of high momentum components in the wave function, that play an important role in the evaluation of transition and elastic form factors ⁹ and in the large x region in DIS ¹.

The relevant effects of relativistic covariance are more evident looking at the polarized distributions $\Delta u_V(x, \mu_0^2) \equiv g_1^u(x, \mu_0^2)$, $\Delta d_V(x, \mu_0^2) \equiv g_1^d(x, \mu_0^2)$ where the spin dynamics on the light-front plays a crucial role (Fig. 1). The introduction of the Melosh rotations results in a substantial enhancement of the responses at large x and in an suppression of the response for $0.1 \lesssim x \lesssim 0.5$ as can be seen from Fig. 1. We show, in the same figure, also the predictions of a pure relativized solution obtained by solving numerically Eq. (4) and neglecting the Melosh rotation effects in (8) (dotted curves). Such a calculation retains the contribution due to the high momentum components, while the covariance requirement on the parton distribution is lost.

3 Results

We shall give results in two scenarios characterized by different gluon distributions (ΔG) at the hadronic scale:

- i) Scenario A : $\Delta G(x, \mu_0^2) = 0$. Only quark valence distributions are allowed at the hadronic scale. The momentum sum rule determines $\mu_0^2 = 0.094$

GeV² at NLO ($[\alpha_s(\mu_0^2)/(4\pi)]_{\text{NLO}} = 0.142$)¹⁰.

- ii) Scenario B: $\Delta G(x, \mu_0^2) = f G(x, \mu_0^2)$. f is the fraction of polarized gluons and has to be considered with the appropriate sign.

A natural choice for the unpolarized gluon distribution within the present approach, has been discussed in refs.^{1,10} and assumes a *valence-like* form $G(x, \mu_0^2) = \frac{N_g}{3} [u_V(x, \mu_0^2) + d_V(x, \mu_0^2)]$. This definition implies $\int G(x, \mu_0^2) dx = 2$ and therefore only 60% of the total momentum is carried by the valence quarks at the scale μ_0^2 . In this case $\mu_0^2 = 0.220$ GeV² at NLO ($[\alpha_s(\mu_0^2)/(4\pi)]_{\text{NLO}} = 0.053$). If the gluons are fully polarized one has $|\Delta G(x, \mu_0^2)| = G(x, \mu_0^2)$. Jaffe's suggestion¹¹ in our approximation implies $\Delta G(x, \mu_0^2) \approx -0.35 G(x, \mu_0^2)$ ^a.

In Fig. 2 the results for the proton structure function $g_1^p(x, Q^2) = \frac{1}{2} \sum_a e_a^2 (g_1^a(x, Q^2) + g_1^{\bar{a}}(x, Q^2))$ are shown and compared with the experimental data. The non-relativistic approximation of the present calculation appears to reproduce rather poorly the experimental observations. Even the use of non-relativistic models which reproduce rather well the baryon spectrum does not alter this conclusion, as shown in ref.¹⁰.

The full covariant calculation leads to theoretical predictions quite close to experimental data in the region $0.01 \lesssim x \lesssim 0.4$ under the assumption of a pure valence component at the hadronic scale (scenario A). The calculation is parameter-free and the only adjustable parameters (τ and κ_l in Eq. (4)) have been fixed to reproduce the low-lying nucleon spectrum as discussed in the previous section. The effect of relativistic covariance in the quark wave function is mainly associated to the spin dynamics induced by the Melosh rotations (8)⁴ and these transformations lead to a strong suppression of this structure function in the small- x region ($x \lesssim 0.5$).

In order to introduce the gluons non perturbatively we evolve the unpolarized distributions predicted by the scenario A, up to the scale of scenario B where 60% of the total momentum is carried by valence quarks. At that scale we substitute the bremsstrahlung gluons by the valence gluons as defined previously. Moreover, at that scale the fraction of polarized gluons is chosen to be *negative* according to Jaffe's result¹¹. Note that we are maximizing the difference with respect to the radiative gluons, because those lead to a positive polarization. Fig. 2 leads us to conclude that the low- x data on g_1^p do not constrain the gluon polarization strongly. If we vary the fraction of polarized gluons from 35% to 100% the quality of the agreement is deteriorated in the

^aIn fact in ref.¹¹ it has been shown that $\int \Delta G(x, \mu_0^2) dx < 0$. Such inequality does not imply $\Delta G(x, \mu_0^2) < 0$ in the whole x -range.

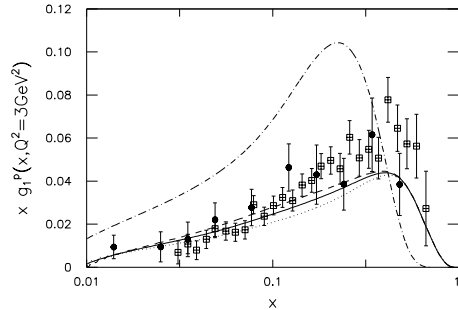


Figure 2: The proton polarized structure function at $Q^2 = 3 \text{ GeV}^2$. The full curve represents the NLO (\overline{MS}) results of a complete light-front calculation within a scenario where no gluons are present at the hadronic scale (scenario A); the corresponding non-relativistic calculation are shown by the dot-dashed line. Scenario B is summarized by the dotted line in the case of negative polarized gluon fraction ($\int \Delta G = -0.7$ as discussed in the text), and by the dashed line in the case of positive gluon polarization ($\int \Delta G = +0.7$). Data are from SMC¹², and SLAC(E142)¹³ experiments.

region $0.01 \lesssim x \lesssim 0.4$, but only slightly. For larger values of x the valence contribution plays a major role and the behavior of the structure functions depends largely on the model wave functions.

Concerning the gluon distribution, our results are summarized in Fig. 3. Within scenario A the polarized gluon distributions remain *positive* at the experimental scale as a result of the NLO evolution. On the contrary a large amount of *negative* gluon polarization is predicted within scenario B if one assumes anti-aligned gluons at the hadronic scale. The distribution is largely dependent on the polarization fraction. The dotted line of Fig. 3a shows the consequence, in the deep inelastic regime, of the Jaffe's calculation at low energy. The absence of non-perturbative sea polarization results in a huge (and probably unrealistic) amount of negative gluon polarization to reproduce the neutron data. Such a large amount of gluons is, however, inconsistent with the unpolarized gluon distributions as it is shown in Fig. 3b (dotted line again).

4 Transversity and Relativistic Spin Effects

In addition to the unpolarized and helicity parton distributions, a third parton distribution, the so called transversity $h_1(x, Q^2)$, is required to get a complete twist-2 description of the momentum and spin structure of the nucleon¹⁵. As the most remarkable feature h_1 is chiral-odd and as a consequence it decouples from electron-nucleon DIS and other easily accessible hard processes. In doubly

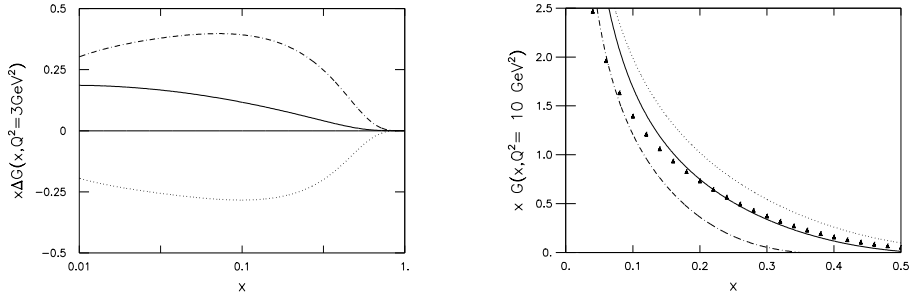


Figure 3: Left panel: Polarized gluon distributions at $Q^2 = 3 \text{ GeV}^2$ obtained evolving at NLO (\overline{MS}) the polarized partons in both scenarios. Scenario A (full line). Scenario B is summarized by the dotted line in the case of negative polarized gluon fraction ($\int \Delta G(x, \mu_0^2) = -0.7$ as discussed in the text), and by the dot-dashed line in the case of positive gluon polarization ($\int \Delta G(x, \mu_0^2) = +0.7$). Right panel: unpolarized gluon distribution at $Q^2 = 10 \text{ GeV}^2$ obtained evolving at NLO (DIS) unpolarized partons. Scenario A (full line); scenario B (dotted line). For comparison also the results at LO are shown in this case (dot-dashed). CTEQ4 NLO (DIS) fit of ref. ¹⁴: full triangles.

polarized Drell-Yan processes ($\vec{p}\vec{p} \rightarrow l^+l^-X$) the chirality of the partons that annihilate is uncorrelated and, in principle, h_1 could be measured (experiments are already included in the research program at HERA and RHIC ¹⁶).

We will focus on an observable defined as the ratio between double transverse and double longitudinal asymmetry in the cross section:

$$R(x_1, x_2, Q^2) \equiv \frac{A_{TT}}{A_{LL}} \frac{1}{f(\theta, \phi)} = \frac{\sum_a e_a^2 h_1^a(x_1, Q^2) h_1^{\bar{a}}(x_2, Q^2) + (x_1 \leftrightarrow x_2)}{\sum_a e_a^2 g_1^a(x_1, Q^2) g_1^{\bar{a}}(x_2, Q^2) + (x_1 \leftrightarrow x_2)} \quad (11)$$

where $f(\theta, \phi)$ is a function of the angles of the final detected lepton, a indicates the flavor of the parton, Q^2 is the invariant mass of the produced pair and the variables x_1 and x_2 are defined in terms of Q^2 , the center of mass energy \sqrt{s} and the quantity $y = \text{arcth}(Q^3/Q^0)$:

$$x_1 = \sqrt{\frac{Q^2}{s}} e^y, \quad x_2 = \sqrt{\frac{Q^2}{s}} e^{-y} \quad (12)$$

The physical meaning of h_1 is similar to that of g_1 but in a transverse basis. It is clear that in any non-relativistic description of the nucleon, where motion and spin commutes, $h_1^a(x, \mu_0^2) = g_1^a(x, \mu_0^2)$ at the hadronic scale μ_0 . However, Melosh rotation is able to break this degeneracy and $h_1(x, \mu_0^2)$ can be

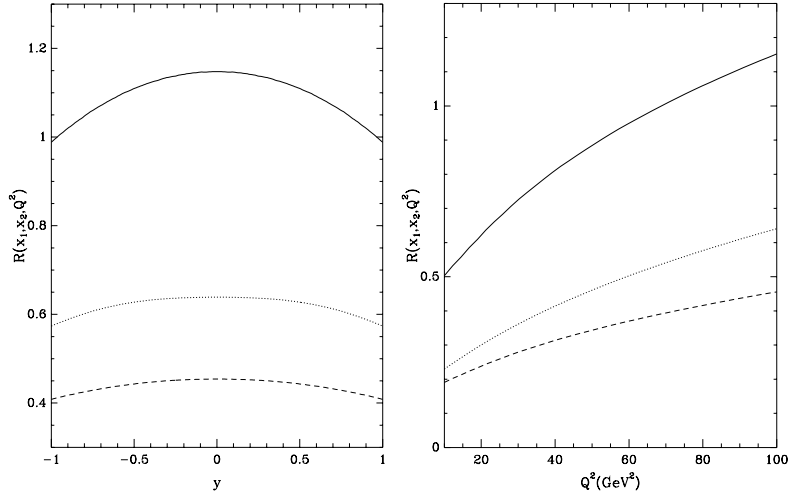


Figure 4: Ratio between transverse and longitudinal asymmetries (eq (11)) as a function a) of the center of mass rapidity y for $Q^2 = 100 \text{ GeV}^2$ and a center of mass energy $\sqrt{s} = 100 \text{ GeV}$ (solid line); b) of the invariant mass of the produced lepton pair (Q^2) for a center of mass rapidity $y = 0$ and a center of mass energy $\sqrt{s} = 100 \text{ GeV}$. The dashed line corresponds to the case when the Melosh rotation is switched off. The dotted line is the result obtained in a fully non-relativistic approach.

expressed in the same form as $g_1(x, \mu_0^2)$, eq. (8), but with different coefficients: $B_u = 4, C_u = 0$ and $B_d = -1, C_d = 0$ ¹⁷.

By employing the wave functions calculated in the previous sections and NLO evolution we have calculated $R(x_1, x_2, Q^2)$ at a scale $Q^2 = 100 \text{ GeV}^2$ (Fig. 4a). Comparing the curves shown in Fig. 4a it is clear that if MR is not taken into account, i.e. we start from the equality $h_1^a(x, \mu_0^2) = g_1^a(x, \mu_0^2)$, the obtained value for R is approximately a factor 2 smaller than when MR is considered. The same conclusion holds for a wide kinematic regimen (see Fig. 4b). Furthermore, the chosen observable is quite insensitive to the details of the mass operator. To check the dependence on the chosen spatial wave function we have recalculated $R(x_1, x_2, Q^2)$ with the non-relativistic version of the mass equation (4) and results are also shown in Fig. 4. Therefore we can conclude that the chosen observables is a rather direct measure of the importance of relativistic spin effects in the nucleon (MR) while it is quite insensitive to the details of the spatial wave function.

Acknowledgments

We acknowledge useful conversations with S. Scopetta regarding factorization schemes. This work has been supported in part by DGICYT-PB94-0080 and the TMR programme of the European Commission ERB FMRX-CT96-008.

References

1. M. Traini, A. Zambarda and V. Vento, *Mod. Phys. Lett.* **10**, 1235 (1995); M. Traini, V. Vento, A. Mair and A. Zambarda, *Nucl. Phys. A* **614**, 472 (1997).
2. G. Parisi and R. Petronzio, *Phys. Lett. B* **62**, 331 (1976).
3. R.L. Jaffe and G.C. Ross, *Phys. Lett. B* **93**, 313 (1980).
4. P. Faccioli, M. Traini and V. Vento, hep-ph/9808201 (to appear in *Nucl. Phys. A*).
5. F. Coester, *Progr. Part. Nucl. Phys.* **29** (1992) 1; J. Carbonell, B. Deplanques, V.A. Karmanov and J.-F. Mathiot, *Phys. Rep.* **300**, 215 (1998); S.J. Brodsky, H.C. Pauli and S.S. Pinsky, *Phys. Rep.* **301**, 299 (1998).
6. H.J. Melosh, *Phys. Rev. D* **9**, 1095 (1974).
7. M. Ferraris, M.M. Giannini, M. Pizzo, E. Santopinto and L. Tiator, *Phys. Lett. B* **364**, 231 (1995).
8. F. Coester, K. Dannbom and D.O. Riska, *Nucl. Phys. A* **634**, 335 (1998).
9. F. Cardarelli, E. Pace, G. Salmè and S. Simula, *Phys. Lett. B* **357**, 267 (1995); *Phys. Lett. B* **371**, 7 (1996).
10. A. Mair and M. Traini, *Nucl. Phys. A* **624**, 564 (1997); *Nucl. Phys. A* **628**, 296 (1998).
11. R.L. Jaffe, *Phys. Lett. B* **365**, 359 (1996).
12. B. Adeva *et al.* (SMC), *Phys. Lett. B* **302**, 533 (1993); *Phys. Lett. B* **329**, 399 (1994); D. Adams *et al.* (SMC), *Phys. Lett. B* **357**, 248 (1995).
13. P.L. Anthony *et al.* (E142), *Phys. Rev. Lett.* **71**, 959 (1993); K. Abe *et al.* (E143), *Phys. Rev. Lett.* **74**, 346 (1995); *Phys. Rev. Lett.* **75**, 25 (1995).
14. CTEQ Collab. H.I. Lai *et al.*, *Phys. Rev. D* **51**, 4763 (1995); *Phys. Rev. D* **55**, 2862 (1997).
15. R.L. Jaffe and X. Ji, *Nucl. Phys. B* **375**, 527 (1992) and refs. therein.
16. N. Saito, *Nucl. Phys. A* **638** (1998) 575. M. Anselmino *et al.*, Proc. of the 'Workshop on Future Physics at HERA', Hamburg 1995. hep-ph/9608393.
17. F. Cano, P. Faccioli and M. Traini, hep-ph/9902345.